

# ASCA Observations of the Starburst-Driven Superwind Galaxy NGC 2146: Broad Band (0.6 - 9 keV) Spectral Properties

Roberto Della Ceca<sup>1</sup>, Richard E. Griffiths<sup>2</sup>, Timothy M. Heckman<sup>3</sup>, Matthew D. Lehnert<sup>4</sup>  
and Kimberly A. Weaver<sup>5</sup>

Received : August 4, 1998;    accepted : October 12, 1998

Astrophysical Journal, in press

---

<sup>1</sup>Osservatorio Astronomico di Brera, 20121 Milano, Italy. E-mail: rdc@brera.mi.astro.it

<sup>2</sup>Physics Department, Carnegie Mellon University, Pittsburgh, PA 15213-3890, USA. E-mail: griffith@astro.phys.cmu.edu

<sup>3</sup>Department of Physics and Astronomy, The Johns Hopkins University, Baltimore, MD 21218, USA. E-mail: heckman@eta.pha.jhu.edu

<sup>4</sup>Sterrewacht Leiden, Postbus 9513, 2300 RA Leiden, The Netherlands. E-mail: lehnert@strw.leidenuniv.nl

<sup>5</sup>NASA/Goddard Space Flight Center, Code 662, Greenbelt, Maryland 20771, USA. E-mail: kweaver@milkyway.gsfc.nasa.gov

## ABSTRACT

We report ASCA GIS and SIS observations of the nearby ( $D = 11.6$  Mpc), nearly edge-on, starburst galaxy NGC 2146. These X-ray spectral data complement ROSAT PSPC and HRI imaging discussed by Armus et al., 1995.

The broad band (0.6-9 keV) X-ray spectrum of NGC 2146 is best described by a two component model: the soft X-ray emission with a Raymond-Smith thermal plasma model having a temperature of  $kT \sim 0.8$  keV; the hard X-ray emission with a thermal plasma model having  $kT \sim 8$  keV or a power-law model having a photon index of  $\sim 1.7$ . We do not find compelling evidence of substantial excess absorption above the Galactic value. The total luminosities of NGC 2146 in the soft (0.5 - 2.0 keV), hard (2-10 keV) and broad (0.5-10.0 keV) energy bands are  $\sim 1.3 \times 10^{40}$ ,  $\sim 1.8 \times 10^{40}$  and  $\sim 3.1 \times 10^{40}$  ergs  $\text{sec}^{-1}$ , respectively. The soft (hard) thermal component provides about 30% (70%) of the total luminosity in the 0.5 - 2.0 keV energy band, while in the 2-10 keV energy range only the hard component plays a major role.

The spectral results allow us to set tighter constraints on the starburst-driven superwind model, which we show can satisfactorily account for the luminosity, mass, and energy content represented by the soft X-ray spectral component. We estimate that the mass outflow rate ( $\sim 9 M_{\odot}$  per year) is about an order of magnitude greater than the predicted rate at which supernovae and stellar winds return mass into the interstellar medium and, therefore, argue that the flow is strongly “mass-loaded” with material in and around the starburst. The estimated outflow velocity of the hot gas is close to the escape velocity from the galaxy, so the fate of the gas is not clear. We suggest that the hard X-ray spectral component is due to the combined emission of X-ray binaries and/or young supernovae remnants associated with the starburst.

*Subject headings:* galaxies: evolution - galaxies: interstellar medium - galaxies:  
starburst - galaxies: intergalactic medium - X-rays: galaxies

## 1. Introduction

In the past few years there has been increasing theoretical and observational evidence demonstrating that the collective effect of multiple supernovae and stellar winds in starburst galaxies can drive a galactic-scale outflow of gas, hereafter a “superwind”. Such phenomena have been hypothesized to be the mechanism whereby proto-elliptical galaxies and bulges are cleared of their nascent interstellar medium, to be responsible for establishing the metallicity-radius relation or the mass-metallicity relation among galaxies, and for chemically-enriching and heating the inter-galactic medium (see Heckman, Lehnert and Armus, 1993; Bland-Hawthorn 1995 for recent reviews). The study of this process is therefore of fundamental importance for understanding many areas of current observational cosmology. Optical and radio observations can provide only indirect evidence of superwind. On the contrary, X-rays directly probe the physical condition of the hot wind material. Such data thus play a key role in the detection, study and investigation of the process of starburst-driven outflows.

NGC 2146 is a nearby (D=11.6 Mpc, at this distance  $1' \simeq 3.37$  kpc) SB(s)ab, nearly edge-on ( $i \sim 63^\circ$ ), starburst galaxy with multi-wavelength evidence for driving a “superwind”. The absolute magnitude of NGC 2146 is  $M_B = -19.2$  ( $B_T = 11.38$ ;  $L_B \simeq 7.5 \times 10^9 L_{B,\odot}$ ); the optical size of the galaxy (at the limiting surface brightness of 25 B magnitude per square arcsec, after correction for Galactic extinction) is about  $6.0 \times 3.4$  arcmin ( $\simeq 20.2 \times 11.5$  kpc); the position angle of the major axis is about  $56^\circ$  (de Vaucouleurs et al., 1991). Its large  $H_\alpha$  luminosity ( $L_{H_\alpha} \simeq 1.5 \times 10^{41}$  ergs sec $^{-1}$ ) and strong, warm infrared emission ( $L_{(1-1000\mu m)} \simeq 1.5 \times 10^{44}$  ergs sec $^{-1}$ ;  $S_{(60\mu m)} \sim 0.76 S_{(100\mu m)}$ ) are similar to those observed in other starburst galaxies with suspected “superwind” activity (see Lehnert and Heckman, 1995; 1996 and references therein). Armus et al., 1995 (hereafter A95) discuss in detail the “superwind” hypothesis by using optical broad and narrow  $H_\alpha$

images, long-slit optical spectra, 6 cm radio data and X-ray (ROSAT PSPC and ROSAT HRI) data. We summarize below the X-ray properties of this galaxy as derived from the ROSAT PSPC and HRI data.

The ROSAT PSPC image ( $E \simeq 0.2-2.4$  keV) show a large X-ray nebula with a half-light diameter of  $\sim 1'$  ( $\sim 3.37$  kpc), a maximum size of  $\sim 4'$  ( $\sim 13.5$  kpc) and a total unabsorbed flux (luminosity) of  $f_{x_{0.2-2.4\text{keV}}} = 1.1 \times 10^{-12}$  ergs  $\text{cm}^{-2}$   $\text{sec}^{-1}$  ( $L_{x_{0.2-2.4\text{keV}}} \simeq 1.8 \times 10^{40}$  ergs  $\text{sec}^{-1}$ ). This nebula, that extends well beyond the starburst in the NE-SW direction (approximately along the minor axis of NGC 2146), is much larger than the starburst ridge seen at 6 cm and seems to be associated with a region of  $H_\alpha$  and dust filaments seen in optical images; it probably traces the expanding superwind. The inner ( $< 0.5'$ ) X-ray nebula is resolved by the ROSAT HRI into at least four point sources, a nuclear “spur”, and strong diffuse emission over the central arcminute. The X-ray “spur” follows the same position angle along the optical major axis as the 6cm radio ridge. The four resolved point sources account for 30% – 50% of the total flux in the HRI. The ROSAT PSPC X-ray spectrum is best described by a soft thermal plasma (kT  $\sim 0.4 - 0.5$  keV) plus a “high energy” component consistent with either a power law (photon index =1.7) or a thermal bremsstrahlung (kT  $> 5$  keV), which dominates above 1 keV. However, the limited energy range and spectral resolution of the ROSAT PSPC prevents a detailed investigation of the X-ray spectral properties of NGC 2146.

For this reason we observed NGC 2146 with ASCA with the specific aims of: a) verifying spectroscopically the presence of multiple components in the X-ray emission; b) measuring their respective luminosities; c) evaluating their proportional contribution in the soft ( $E < 2$  keV) and hard ( $E > 2$  keV) energy bands and, therefore, d) setting tighter constraints on the starburst-driven superwind model.

This paper is organized as follows. In section 2 we present the ASCA data; their

spectral analysis is reported in section 3. Section 4 contains a discussion of the results. Finally, a summary of our conclusions is presented in section 5.

## 2. ASCA Observations and data preparation

NGC 2146 was observed on March 26, 1997 by the ASCA satellite (Tanaka, Inoue and Holt, 1994). The spectral data were extracted using version 1.3 of the XSELECT software package and version 4.0 of FTOOLS (supplied by the HEASARC at the Goddard Space Flight Center). Good time intervals were selected by applying the “Standard REV2 Screening” criteria as reported in chapter 5 of the ASCA Data Reduction Guide (rev 2.0). For the GIS instruments we have combined HIGH, MEDIUM and LOW bit rate data; for the SIS instruments we have combined HIGH and MEDIUM bit rate data. The SIS was operated in 1 CCD ‘Bright’ and ‘Faint’ modes during the observation. Faint mode data were converted to Bright mode and Hot and Flickering pixels were removed. From an inspection of the light curves, we also rejected times of high count rate due to background variations. The total effective exposure time was 60938 sec for SIS0, 60817 sec for SIS1 and 66417 sec for GIS2 and GIS3.

Source counts were extracted from a circular region around the centroid of X-ray emission from NGC 2146. This region has a 3.6 arcmin radius for SIS0 and SIS1 (the maximum allowed due to the position of NGC 2146 within the CCD chips) and a 6 arcmin radius for GIS2 and GIS3. For the SIS, background counts were taken from source-free rectangular regions within the CCD chip that contained NGC 2146. For the GIS, background counts were taken from source-free circular regions close to NGC 2146. Source and background counts were extracted in the “Pulse Invariant” (PI) energy channels, which have been corrected for spatial and temporal variations of the detector gain. We

also checked several regions for differences in the background counting rate, but found no significant spatial variations. The total net counts (hereafter “net counts” refer to the background subtracted counts) from NGC 2146 are  $\sim 2150$  for SIS0,  $\sim 1900$  for SIS1,  $\sim 1700$  for GIS2 and  $\sim 2100$  for GIS3. The net counts represent about 67% (SIS0,SIS1) and 58% (GIS2,GIS3) of the total gross counts in the source region.

We exclude from the spectral analysis all data with  $E > 9$  keV and  $E < 0.6$  keV. The upper limit is chosen because background dominates at these energies; the lower limit is chosen because the GIS data do not provide sufficient statistics and because the SIS calibration is not well known below this energy due to an ill-defined modeling of the O K edge in the response matrix (see Dotani et al., 1996) and uncertainties in the corrections for the loss of photons due to charge transfer. For the GIS data we use the detector Redistribution Matrix Files (RMF) `gis2v4_0.rmf` and `gis3v4_0.rmf`, respectively. For the SIS data the RMF files were obtained using the FTOOLS task `SISRMG`. The Ancillary Response Files (ARF) were created with the version 2.72 of the FTOOLS task `ASCAARF` at the location of NGC 2146 in the detectors (see George et al., 1992 for the definition of the RMF and ARF calibration files).

In order to improve the statistics we produce a combined SIS spectrum (SIS 0 and SIS 1 were added, S01 hereafter) and a combined GIS spectrum (G23 hereafter). The combined spectra and their respective background and response matrix files have been obtained following the recipe given in the ASCA Data Reduction (rev 2.0) Guide (see sections 8.9.2 and 8.9.3 and reference therein). In order to use  $\chi^2$  statistic in the spectral fitting procedure (see Section 3), S01 and G23 were rebinned to give at least 30 total counts (source + background) per energy bin.

In section 3 we also use the ROSAT PSPC data in order to test for intrinsic (i.e. inside NGC 2146) soft X-ray absorption. NGC 2146 was observed with the PSPC in pointed mode

(with the object at the center of the detector) on 1992 February 25 for a total exposure time of 5799 sec. The data were retrieved from the ROSAT archive (ROR=700440). Source counts were extracted from a circular region of  $\sim 2.5$  arcmin radius around the centroid of X-ray emission from NGC 2146. Background counts were extracted from an annular region of inner radius  $\sim 6$  arcmin and outer radius  $\sim 8$  arcmin around NGC 2146. A total of about 400 net counts were accumulated from the source. All data with an energy above 0.2 keV were included in the spectral analysis; the PSPC spectrum was rebinned to give at least 15 net counts per bin. It is worth noting that these data are the same as used by A95.

Spectral analysis (see Section 3) has been performed using version 9.0 of the XSPEC software package (Arnaud, 1996). The SIS and GIS data are fitted jointly and the model normalization(s) for each data set are allowed to be an independent parameter in order to take into account differences in the absolute calibration of the instruments.

### 3. Spectral Analysis

X-ray observations of the brightest starburst galaxies (e.g. NGC 253 and M82, Moran and Lehnert, 1997; Ptak et al., 1997; Dahlem, Weaver and Heckman 1998; Persic et al., 1998; NGC 3310 and NGC 3690, Zezas, Georgantopoulos and Ward, 1998) as well as of low-mass star-forming systems (e.g. NGC 1569 and NGC 4449; Della Ceca et al., 1996; Della Ceca, Griffiths and Heckman, 1997) have shown that the X-ray spectra of this class of objects are very complex, displaying at least two or three spectral components. This is not surprising given that X-rays from starburst galaxies are expected to derive from different classes of sources like stars, accreting binary star systems, supernova remnants, diffuse hot gas and outflowing winds, and inverse Compton emission.

Single-component models do not provide an adequate description of NGC 2146. A



single-temperature thermal model (Raymond-Smith or Mekal) and a single power law model, both modified by Galactic absorption ( $N_{H_{Gal}} = 7.3 \times 10^{20} \text{ cm}^{-2}$ , see A95) are rejected at a high confidence level ( $\geq 99.99\%$ ). For the thermal models, the abundance of the X-ray emitting gas is fixed at the solar value. Allowing  $N_H$  and/or the abundance of the X-ray emitting gas to vary as free parameters (with the condition  $N_{H_{fit}} > N_{H_{Gal}}$ ) does not produce a better fit. From the visual inspection of the residuals to the best fit Raymond-Smith model for each detector (see Figure 1) we note that the largest discrepancies are not concentrated around expected emission lines, as in the case of the high signal-to-noise SIS spectra of M82 reported and discussed in Moran and Lehnert (1997). Rather, discrepancies occur in the shape of the spectrum for  $E \lesssim 2 \text{ keV}$ , which is a clear indication that a more complex spectrum is needed to describe the X-ray spectral properties of NGC 2146. Similar results are obtained for the power-law model or for the Mekal model.

We then tried the following two-component spectral models: 1) a two-temperature Raymond-Smith model (hereafter the Ray+Ray model) and 2) a Raymond-Smith model plus a power law model (hereafter the Ray+Po model). These trial models were filtered by Galactic absorption ( $N_{H_{Gal}} = 7.3 \times 10^{20} \text{ cm}^{-2}$ ); the abundance of the X-ray emitting gas was fixed at the solar value. The results are reported in Table 1; the folded spectra and the residuals to the best fit Ray+Po model for each detector are displayed in Figures 2 (G23) and 3 (S01). Similar results are obtained for the Ray+Ray model. As evident from the residuals shown in Figures 2 and 3 and from the  $\chi^2_\nu$  in Table 1, both models are a good representation of the ASCA data. The spectral parameters derived from single-instrument fits are in good agreement, within the respective errors, with those obtained from the joint SIS+GIS fits. We also obtain similar results if we replace the Raymond-Smith thermal model with the Mekal thermal model, showing that the fits are insensitive to the detailed physics of the model.

In order to test for the presence of intrinsic absorption, we include the ROSAT PSPC data in the spectral analysis; the inclusion of these data allows us to extend the coverage of the NGC 2146 X-ray spectra down to  $E \sim 0.2 - 0.3$  keV. The combined ASCA+ROSAT PSPC data set are fitted with the two-component models discussed above but the absorbing column density is left as a free parameter. The results are reported in Table 1. The best fit spectral parameters are in good agreement with those derived from ASCA alone; furthermore the absorbing column density along the line of sight is not significantly in excess above the Galactic value.

Moran and Lehnert (1997) by studying the high quality ASCA + ROSAT PSPC data of the prototype starburst galaxy M82 have found that the (0.1 - 10 keV) spectrum of this galaxy is best described by a three components model composed of: a) a very soft Raymond-Smith thermal component with  $kT \simeq 0.3$  keV; b) an absorbed Raymond-Smith thermal component with  $kT \simeq 0.6$  keV and c) a heavily absorbed ( $N_H \sim 10^{22}$  cm<sup>-2</sup>) hard component that can be described either by a power-law with photon index equal to 1.7 or by a thermal bremsstrahlung with  $kT \simeq 18$  keV. The observed 0.1-10 keV flux from M82 is dominated from this latter component. We have tried to fit the ASCA + ROSAT PSPC data of NGC 2146 using a different absorbing column density for the hard component. The best fit spectral parameters for the original two components model(s) are in very good agreement with those reported in Table 1, the absorbing column density of the hard component is consistent with zero and the  $\chi^2$  is not improved with the inclusion of this additional parameter. So, with the current statistic we are unable to determine the possible excess absorption of the hard component, as found by Moran and Lehnert (1997) for M82.

Finally, we have also tried to fit the ASCA + ROSAT PSPC data with the abundance as free parameter for the soft component; unfortunately our data are not able to set any useful constraint on the abundance.

To summarize, the broad band X-ray spectrum of NGC 2146 reveals the presence of at least two spectral components: the soft component is best described by a Raymond-Smith thermal model with a temperature of  $\sim 0.8$  keV, while the hard component can be described by a thermal model with a temperature of  $\sim 8$  keV or by a power-law model with photon index of  $\sim 1.7$ . There is no compelling evidence of intrinsic absorption inside NGC 2146. The unfolded spectrum of the ASCA + ROSAT PSPC data set (Ray+Po spectral model) is shown in Figure 4.

We stress that the two-component spectral models reported above must be considered as a “first order” approximation of the real spectral energy distribution in NGC 2146. As already discussed at the beginning of section 3, X-ray emission from starburst galaxies is expected to derive from several processes and several locations; therefore, more complex X-ray spectra should be considered more realistic. These are the limitations of the current data sets. Spatially resolved spectroscopy will be possible with the instrumentation on board AXAF, JET-X and XMM, allowing us to investigate in deeper detail the spectral properties of NGC 2146 and similar objects.

## 4. Discussion

### 4.1. Fluxes and Luminosities

We report in Table 2 the unabsorbed X-ray fluxes and luminosities of the spectral components in the soft (0.5 - 2.0 keV) and hard (2.0 - 10.0 keV) energy range for the two spectral models discussed above. For the normalization of the spectral components we have used a mean value between the G23 and the S01 normalizations (see Table 1). The total unabsorbed luminosity of NGC 2146 in the soft, hard and broad (0.5-10.0 keV) energy band

is  $\sim 1.3 \times 10^{40}$ ,  $\sim 1.8 \times 10^{40}$  and  $\sim 3.1 \times 10^{40}$  ergs sec $^{-1}$ , respectively. The soft (hard) X-ray component provides about 30% (70%) of the total flux in the soft energy band. Almost all ( $> 98\%$ ) the flux in the 2 - 10 keV energy band is produced by the hard spectral component. Given the uncertainties on normalizations, the fluxes and luminosities reported in Table 2 are estimated to be correct to about 30%.

## 4.2. The Soft X-ray Emitting Gas

### 4.2.1. Physical Parameters

The straightforward interpretation of the origin of the soft X-ray spectral component is to associate it with the diffuse X-ray emitting gas that has been detected with the ROSAT PSPC and HRI data by A95.

The best fit spectral parameters reported in Table 1 allow us to determine the basic physical conditions of this X-ray emitting gas. For a gas with a temperature of  $\sim 0.8$  keV and a normalization of  $\sim 1 \times 10^{-4}$  at 1 keV <sup>6</sup> (a mean value between the normalizations reported in Table 2), the emission integral (EI =  $\int n_e^2 dV$ ) is equal to  $1.61 \times 10^{62}$  cm $^{-3}$ .

For consistency we will adopt the same geometry as A95: namely, half of the emission integral is represented by gas interior to a radius of  $\sim 0.5' \simeq 1.69$  kpc (the “inner region”) and the remaining is represented by the gas located between radii of  $\sim 0.5'$  and  $\sim 2.5'$ , or 1.69 - 8.43 kpc (the “outer region”).

---

<sup>6</sup> This number is equal to  $[10^{-14}/(4\pi D^2)] \int n_e^2 dV$ , where D is the distance to the source in cm,  $n_e$  is the electron density in units of cm $^{-3}$  and V is the volume filled by the X-ray emitting gas in cm $^3$ .

Parameterizing the clumpiness of the gas by a volume ( $V$ ) filling factor  $f$ , we can determine: the gas density ( $n_e \sim (\frac{E.L.}{V.f})^{1/2}$ ), the gas pressure ( $p \sim 2 n_e k T$ ), the gas mass ( $M \sim n_e m_p V f$ ), the thermal energy of the gas ( $E \sim 3 n_e k T V$ ) and the radiative cooling time ( $t_{cool} \sim \frac{3 k T}{\Lambda n_e}$ ), where  $T$  is the temperature of the gas and  $\Lambda$  is the emissivity of the gas. In computing the radiative cooling time we have taken  $\Lambda = 2.0 \times 10^{-23} \text{ erg cm}^3 \text{ s}^{-1}$  which is appropriate for gas in collisional ionization equilibrium with solar abundances and a temperature of 0.8 keV (Sutherland and Dopita 1993). The physical parameters of the soft X-ray emission implied by the best fit spectral model, in the “inner” and the “outer” regions, are reported in Table 3.

We note that an increase of a factor 2 of the spectral normalization implies an increase of a factor 1.41 in the physical parameters of the X-ray emission reported in Table 3 (except for the radiative cooling time, which decreases by the same factor). Therefore the quantities reported in Table 3 can be considered a good order-of-magnitude estimate of the physical conditions of the diffuse soft X-ray emitting gas in NGC 2146.

#### 4.2.2. *The Origin of the Soft X-ray Emission*

We can now compare the above quantities to a simple model to check the assertion of A95 that the soft, spatially-resolved X-ray emission in NGC 2146 is produced by an outflowing superwind. To do so, we will adopt a simple model that assumes that mechanical energy is being continuously injected inside the starburst and used to heat the surrounding gas. This gas then flows out of the starburst and emits X-rays (cf. Wang 1995). In such a model we need to specify the heating rate and the mass-injection rate into the outflow.

We begin by using starburst models of Leitherer and Heckman (1995 - hereafter LH95) to scale the observed bolometric luminosity of NGC 2146 to obtain a predicted rate of

mechanical energy injection (heating). The total IR luminosity of the system is about  $4 \times 10^{10} L_{\odot}$ . The LH95 models then predict a total mechanical luminosity of about  $1.3 \times 10^{42}$  erg s<sup>-1</sup>, and a star-formation rate of  $\sim 5 M_{\odot}$  per year (for a Salpeter IMF extending from 0.1 to 100  $M_{\odot}$ ).

We will assume that the gas in the starburst is initially heated to a temperature of about  $10^7$  K (the temperature of the soft component). For the energy injection rate given above, conservation of energy then implies that gas is heated at a rate of 9  $M_{\odot}$  per year. This is about an order of magnitude greater than the predicted rate at which supernovae and stellar winds return mass to the interstellar medium in this system (cf. LH95). This implies that the outflow is strongly “mass-loaded”: most of the outflowing material is ambient interstellar gas in and around the starburst that has been heated by the supernovae and stellar winds (cf. Suchkov et al 1996). In this case, we would expect the metallicity of the X-ray emitting gas to be similar to that in the interstellar medium of NGC 2146 (see Ptak et al., 1997 and Della Ceca, Griffiths and Heckman, 1997 for similar results on NGC253, M82 and NGC 4449).

Since the energy injection rate of the starburst is several hundred times the X-ray luminosity of the soft component, we will ignore the dynamical effect of radiative cooling in our simple model. This neglect is further justified since the estimated radiative cooling time of the X-ray gas (of order  $10^9$  years - see Table 3) is much longer than the adiabatic expansion timescale (of order  $10^7$  years).

Following Chevalier and Clegg (1985) and Wang (1995) we therefore consider a spherically-symmetric wind with a mass outflow rate of 9  $M_{\odot}$  per year which is “fed” by hot gas that is injected at a uniform temperature of  $10^7$  K. We will take the size of the energy injection region to be similar to that of the central radio source and the bright X-ray emission in the ROSAT HRI data in A95 (radius  $\sim 1$  kpc). The wind reaches a terminal

velocity of  $v_{wind} = 660 \text{ km s}^{-1}$  (Chevalier and Clegg 1985) and cools through adiabatic expansion while also emitting soft X-rays. The emissivity of gas in the 0.1 to 2.2 keV energy band is constant to within about a factor of two as a function of temperature over the range between  $8 \times 10^5 \text{ K}$  to  $10^7 \text{ K}$  ( $\simeq 2 \times 10^{-23} \text{ erg cm}^3 \text{ s}^{-1}$  for solar metallicity). This then allows us to predict an X-ray luminosity from the outflow of  $\simeq 1 \times 10^{40} \text{ erg s}^{-1}$  from within a region equal in size to the X-ray nebula (radius of  $\sim 7 \text{ Kpc}$ ), plus an additional contribution of  $\simeq 5 \times 10^{39} \text{ erg s}^{-1}$  from the hot gas inside the starburst that feeds the outflow. The total estimated luminosity is about a factor of three larger than the measured luminosity of the soft X-ray component, which we regard as satisfactory agreement for such a simple model. Within the X-ray nebula, the predicted mass of the hot gas will be about  $10^8 M_{\odot}$  and the predicted thermal plus kinetic energy in the outflow will be  $5 \times 10^{56} \text{ ergs}$ . Again, these predicted values agree reasonably well with the derived values for the sum of the inner and outer regions (see Table 3):  $M \simeq 7 \times 10^7 f^{1/2} M_{\odot}$  and  $E_{therm} \simeq 3 \times 10^{56} f^{1/2} \text{ ergs}$ .

Note that a radius of 7 kpc and a wind terminal velocity of  $660 \text{ km s}^{-1}$  corresponds to a dynamical age of order  $10^7$  years (reasonable for a starburst). If the outflow has lasted much longer than this, the total mass and energy in the flow will rise accordingly, but this will comprise material at larger radii ( $> 7 \text{ kpc}$ ). Such material will have a low density and (due to adiabatic cooling) a low temperature, and would therefore not produce significant X-ray emission (cf. Wang 1995).

#### 4.2.3. *The Fate of the Hot Gas*

Having demonstrated that a very simple model can reproduce the gross properties of the soft X-ray emission, we next consider the fate of this outflowing gas. Following Wang et al. (1995), the “escape temperature” for hot gas in a galaxy potential with an escape

velocity  $v_{es}$  is given by:

$$T_{es} \simeq 1.26 \times 10^6 (v_{es}/300 \text{ km s}^{-1})^2 \text{ } ^\circ\text{K}$$

The HI rotation curve of NGC 2146 has an amplitude of  $272 \text{ km s}^{-1}$ . Assuming that NGC 2146 has an isothermal dark matter halo extending to a radius of 100 kpc, the escape velocity (see equation 13 in Heckman et al. (1995)) at  $r = 7 \text{ kpc}$  is about  $740 \text{ km s}^{-1}$  and  $T_{es} = 8 \times 10^6 \text{ K}$ . If the dark matter halo extends out to 300 kpc,  $T_{es}$  rises to  $\sim 10^7 \text{ K}$ . These temperatures are similar to the temperature we measure for the hot gas ( $\simeq 10^7 \text{ K}$ ). The escape velocity is also similar to the estimated terminal velocity for the wind (see above). These rough arguments suggest that the outflowing gas *may* be able to escape the gravitational potential of NGC 2146, and thereby carry metals and kinetic energy out into the inter-galactic medium.

### 4.3. The Origin of the Hard X-ray Emission

A95 discusses the following scenarios for the origin of the hard spectral component: a) thermal emission from the hot wind fluid that is built up in the starburst injection region before the wind expands; b) emission from a population of massive X-ray binaries and/or young supernova remnants in the starburst; c) emission from normal sources not associated with the starburst; d) Inverse Compton emission from the galactic wind and e) an optically obscured active galactic nucleus.

They reach the conclusion that the two most plausible possibilities are Inverse Compton Emission from the galactic wind and emission from a population of massive X-ray binaries and/or young supernova remnants associated with the starburst. We will now discuss these two possibilities.



Low resolution VLA observations of NGC 2146 show a diffuse radio halo surrounding the central starburst; this radio halo is probably produced by synchrotron emission from relativistic electrons that are flowing out of the starburst. Since the starburst also produces a plentiful supply of “soft” (ultraviolet, optical and infrared) photons, inverse Compton scattering of these soft photons by the relativistic electrons will lead to non-thermal X-ray emission from the halo. Furthermore, the hard X-ray spectral component can be satisfactorily described by a power law model (best fit photon index of  $\sim 1.7$ ), which is highly suggestive since this is the X-ray spectral signature of the Compton-scattered photons. It is therefore important to make a rough estimate of the expected inverse Compton luminosity of NGC 2146.

The inverse Compton luminosity ( $L_{IC}$ ) and the Synchrotron luminosity ( $L_{Syn}$ ) are tied together by the relationship,  $L_{IC} = L_{Syn} \times \frac{U_{rad}}{U_B}$ , where  $U_{rad}$  is the energy density of the radiation field and  $U_B (= B^2/8\pi)$  is the energy density of the magnetic field (B).  $U_B$  can be estimated by applying a “minimum” energy calculation (see Moffet, 1975). Input parameters are: a)  $L_{Syn} = 1.53 \times 10^{39}$  ergs sec $^{-1}$ . This latter represents the total radio luminosity (integrated over the frequency range from 10 MHz to 10 GHz) obtained by using a 1.4 GHz flux of  $\sim 1.3$  Jy (White et al., 1992) and assuming a spectral index of 0.7; b) a ratio of total energy of CRs to total energy of electrons  $k=100$ ; c) a volume emitting region approximated by a cylinder with a height of  $\sim 0.8$  kpc and a radius of  $\sim 1.4$  kpc as estimated from the high frequency and high resolution map reported in Lisenfeld et al. (1996). With these assumptions we obtain a magnetic field energy density  $U_B = 1.1 \times 10^{-10}$  erg cm $^{-3}$  ( $B = 52.8 \mu G$ ).  $U_{rad}$  can be computed from the bolometric luminosity,  $U_{rad} = \frac{L_{bol}}{4\pi R^2 c}$ . Since most of the luminosity in NGC 2146 is emitted in the far infrared we will assume  $L_{bol} \simeq L_{1-100\mu m} \simeq 1.5 \times 10^{44}$  ergs sec $^{-1}$ . For the radius R, we will take  $R=1.4$  kpc, which represents the radius of the radio halo. With these assumptions we obtain  $U_{rad} = 2.1 \times 10^{-11}$  erg cm $^{-3}$ . Combining these values we have  $L_{IC:2-10keV} \lesssim 3 \times 10^{38}$

ergs sec<sup>-1</sup>. Therefore it is clear that, unless we are far from the minimum-energy conditions in the radio source, the inverse Compton process will produce only a few percent of the X-ray luminosity of the hard X-ray component. Note that if we use  $k=1$  instead of  $k=100$ , then  $U_B = 1.2 \times 10^{-11}$  erg cm<sup>-3</sup> ( $B = 17.2 \mu G$ ) and  $L_{IC:2-10keV} \lesssim 2.7 \times 10^{39}$  ergs sec<sup>-1</sup>: this is still not enough to produce the hard X-ray emission in NGC 2146.

Excluding inverse Compton emission we are then left with the emission from a population of massive X-ray binaries and/or young supernova remnants associated with the starburst. The total (0.2 - 2.4) keV X-ray flux of the four brightest X-ray sources resolved by the ROSAT HRI in the central starburst of NGC 2146 is  $\sim 3 - 4 \times 10^{-13}$  ergs cm<sup>-2</sup> sec<sup>-1</sup>. The ASCA best fit model(s) imply an (0.2 - 2.4 keV) X-ray flux of the hard component which is a factor two higher than this. Given the uncertainties in the ROSAT HRI fluxes and considering the “first order” nature of the NGC 2146 X-ray spectra, we consider highly plausible that the hard X-ray component represents the combined emission of the “point-like” sources in the starburst. On the other hand, it is worth noting that while massive X-ray binaries and/or young supernova remnants are plausible counterpart of these “point-like” sources, their average spectral properties are different from a power-law model with photon index equal to 1.7 or from a thermal spectrum with  $kT \sim 8$  keV. The massive X-ray binaries have spectra too hard (photon index in the range 0.8-1.5 below 10 keV; Nagase, 1989), while the young supernova remnants are too soft ( $kT \sim 2-3$  keV). The only class of discrete X-ray sources that could have a power-law spectrum with photon index around 1.7 are black-hole binaries in the low state (Tanaka, 1996)<sup>7</sup>. About two to

---

<sup>7</sup> It is worth noting that a power-law spectrum with photon index around 1.7 is also consistent with an AGN hypothesis. However this possibility was discussed and ruled out by A95 on the basis of a) the size of the X-ray nebulae in the 1-2 keV energy range and b) the starburst nuclear spectrum of NGC 2146.

five thousand systems emitting at the low state luminosity (several times  $10^{36}$  ergs  $\text{sec}^{-1}$ ) should be required to take into account of the hard spectral component of NGC 2146. Given that about 1000 (or even more) of such system are estimated to be present in our Galaxy (see Tanaka, 1996), such possibility can not be excluded for a starburst galaxy like NGC 2146.

In summary, while we are confident that the hard X-ray emission is due to the combined emission of the point-like sources associated with the starburst, to understand their physical nature we will have to wait for JETX, AXAF and/or XMM observations.

## 5. Summary and Conclusion

In this paper we have presented and discussed ASCA observations of the starburst galaxy NGC 2146.

The main results of this paper are summarized as follows:

a) The broad band (0.6-9 keV) X-ray spectrum of NGC 2146 is well fitted by a two component model: the soft component can be described by a Raymond-Smith thermal model with a temperature of  $\sim 0.8$  keV, while the hard component can be described by a thermal model with a temperature of  $\sim 8$  keV or by a power-law model with photon index of  $\sim 1.7$ . The  $N_H$  along the line of sight is consistent with the Galactic value. Similar spectral components are found to describe the broad band X-ray spectral properties of other bright starburst galaxies (Ptak et al., 1997; Moran and Lehnert, 1997; Zezas, Georgantopoulos and Ward, 1998; Persic et al., 1998).

b) The total luminosity of NGC 2146 in the soft (0.5 - 2.0 keV), hard (2 - 10 keV), and broad (0.5-10.0 keV) energy band is  $\sim 1.3 \times 10^{40}$ ,  $\sim 1.8 \times 10^{40}$  and  $\sim 3.1 \times 10^{40}$  ergs  $\text{sec}^{-1}$

, respectively. The soft (hard) spectral component provides about 30% (70%) of the total luminosity in the soft 0.5 - 2.0 keV energy band, while in the hard 2-10 keV energy range only the hard spectral component plays a major role.

c) We have shown that a starburst-driven “mass-loaded” superwind model (cf. Suchkov et al., 1996) can satisfactorily account for the gross properties (luminosity, mass, and energy content) of the soft X-ray spectral component. The estimated outflow velocity of the hot gas is close to the escape velocity from the galaxy, so its fate is not clear.

d) We have excluded Inverse Compton emission as the dominant mechanism for the production of the hard spectral component (unless we are far from the minimum-energy conditions in the radio source). We suggest that the hard spectral component is due to the combined emission of massive X-ray binaries and/or young supernova remnants associated with the starburst.

The new ASCA spectral data allowed us to confirm and extend many of the conclusions of A95 (which were based on ROSAT PSPC spectral and imaging data and ROSAT HRI imaging data) in several important ways. First, the broad band (0.6-9 keV) X-ray spectrum of NGC 2146 allows us to verify spectroscopically the presence of multiple components in the X-ray emission, to measure their respective luminosities and to evaluate their proportional contribution in the soft ( $E < 2$  keV) and hard ( $E > 2$  keV) energy bands. Second, using the best fit spectral parameters we have been able to set tighter constraints on the starburst-driven superwind model, in term of mass outflow rate and outflow velocity.

#### Acknowledgments

The authors acknowledge partial financial support from NASA grants NAG5-6400, NAG5-3651 and NAG5-6075. We would like to thank L. Armus and the referee, A. Ptak, for helpful comments and suggestions. This research has made use of the NASA/IPAC

extragalactic database (NED), which is operated by the Jet Propulsion Laboratory, Caltech, under contract with the National Aeronautics and Space Administration. We thank all the members of the ASCA team who operate the satellite and maintain the software data analysis and the archive.

Table 1: Results of the Spectral Fits Using Two Component Models.

Model = Ray+Ray						
Instruments	$kT_{Soft}$	Norm $_{Soft}$	$kT_{Hard}$	Norm $_{Hard}$	$N_H$	$\chi^2_{\nu}/(\text{d.o.f.})$
(1)	(2)	(3)	(4)	(5)	(6)	(7)
G23+S01	$0.82^{0.87}_{0.76}$	$1.59^{2.05}_{1.11}/0.75^{0.97}_{0.49}$	$8.34^{11.76}_{6.05}$	$9.20^{9.99}_{8.44}/7.29^{7.81}_{6.83}$	7.3(fixed)	1.12/252
G23+S01+PSPC	$0.77^{0.86}_{0.66}$	$1.85^{3.65}_{1.08}/0.88^{1.90}_{0.51}/1.65^{3.39}_{0.82}$	$7.07^{11.2}_{5.15}$	$9.41^{10.4}_{8.52}/7.53^{8.34}_{6.93}/6.28^{9.33}_{3.28}$	$13^{41}_{2.5}$	1.12/270

Model = Ray+Po						
Instruments	$kT_{Soft}$	Norm $_{Soft}$	$\Gamma$	Norm $_{Hard}$	$N_H$	$\chi^2_{\nu}/(\text{d.o.f.})$
(1)	(2)	(3)	(4)	(5)	(6)	(7)
G23+S01	$0.82^{0.89}_{0.70}$	$1.29^{1.79}_{0.82}/0.57^{0.80}_{0.32}$	$1.68^{1.79}_{1.57}$	$3.00^{3.40}_{2.50}/2.31^{2.58}_{2.05}$	7.3(fixed)	1.09/252
G23+S01+PSPC	$0.73^{0.83}_{0.62}$	$1.96^{7.00}_{1.08}/0.95^{4.20}_{0.45}/1.86^{6.97}_{0.93}$	$1.79^{1.94}_{1.64}$	$3.43^{4.09}_{2.95}/2.67^{3.21}_{2.25}/2.11^{3.23}_{1.17}$	$21^{43}_{10}$	1.06/270

**Note.** — The elemental abundances in these fits have been fixed at the Solar values. Allowed ranges are at 90% confidence intervals for two interesting parameters ( $\chi^2_{min} + 4.61$ ). Columns are as follows: (1) Instrument; (2) Best fit and 90% confidence interval for the temperature of the soft component in keV; (3) Best fit and 90% confidence interval for the normalization of the soft component at 1 keV in units of  $10^{-4}$  for the G23, S01 and PSPC data set respectively. This number is equal to  $[10^{-14}/(4\pi D^2)] \int n_e^2 dV$ , where D is the distance to the source in cm,  $n_e$  is the electron density in units of  $\text{cm}^{-3}$  and V is the volume filled by the X-ray emitting gas in  $\text{cm}^3$ . (4) Best fit and 90% confidence interval for the temperature of the hard component (Ray+Ray model) in keV or for the power law photon index (Ray+Po model); (5) Best fit and 90% confidence interval for the normalization of the hard component at 1 keV in units of  $10^{-4}$  (Ray+Ray model) or for the normalization of the power law component in units of  $10^{-4}$  photons  $\text{s}^{-1} \text{cm}^{-2} \text{keV}^{-1}$  at 1 keV (Ray+Po model). G23, S01 and PSPC data set, respectively. (6) The absorbing column density along the line of sight in units of  $10^{20} \text{cm}^{-2}$ . (7) Reduced chi-squared and degree of freedom.

Table 2: Unabsorbed X-ray Fluxes and luminosities

Model	$kT_{Soft}$	$Norm_{Soft}$	$F_x(L_x)/F_x(L_x)$ (0.5 - 2.0) keV / (2.0 - 10.0) keV	$kT_{Hard}/\Gamma$	$Norm_{Hard}$	$F_x(L_x)/F_x(L_x)$ (0.5 - 2.0) keV / (2.0 - 10.0) keV
(1)	(2)	(3)	(4)	(5)	(6)	(7)
Ray+Ray	0.82	1.17	2.79 (4.49) / 0.16 (0.26)	8.34	8.25	4.97 (8.00) / 11.38 (18.32)
Ray+Po	0.82	0.93	2.22 (3.57) / 0.13 (0.20)	1.68	2.66	5.96 (9.60) / 11.20 (18.03)

Note. — Columns are as follows: (1) Model; (2) Temperature of the soft component in keV ; (3) Normalization of the soft component at 1 keV in units of  $10^{-4}$ . This number is equal to  $[10^{-14}/(4\pi D^2)] \int n_e^2 dV$ , where D is the distance to the source in cm,  $n_e$  is the electron density in units of  $\text{cm}^{-3}$  and V is the volume filled by the X-ray emitting gas in  $\text{cm}^3$ ; (4) Fluxes and luminosities of the soft spectral component in the (0.5-2.0) keV energy band and in the (2.0 - 10.0) keV energy band. The fluxes are in units of  $10^{-13} \text{ ergs cm}^{-2} \text{ sec}^{-1}$ , while the luminosities are in units of  $10^{39} \text{ ergs sec}^{-1}$ ; (5) Temperature of the hard component (Ray+Ray model) in keV or the power law photon index (Ray+Po model); (6) Normalization of the hard component at 1 keV in units of  $10^{-4}$  (Ray+Ray model) or in units of  $10^{-4} \text{ photons s}^{-1} \text{ cm}^{-2} \text{ keV}^{-1}$  at 1 keV (Ray+Po model); (7) Fluxes and luminosities of the hard spectral component in the (0.5-2.0) keV energy band and in the (2.0 - 10.0) keV energy band. The fluxes are in units of  $10^{-13} \text{ ergs cm}^{-2} \text{ sec}^{-1}$ , while the luminosities are in units of  $10^{39} \text{ ergs sec}^{-1}$ . Numbers reported in column 2 and 5 are the best fit parameters of the combined ASCA data set (with the  $N_H$  held fixed at the Galactic value) for the soft and hard component. respectively. Their corresponding normalizations (column 3 and 6) are mean values between the G23 and S01 normalizations (see Table 1).

Table 3: Physical Conditions and Energetics of the Soft X-ray Emitting Gas

Region	Volume cm <sup>3</sup>	$\langle n_e \rangle$ cm <sup>-3</sup>	$P_x$ dyne cm <sup>-2</sup>	$M_x$ M <sub>⊙</sub>	$E_x$ erg	$t_{cool}$ years
(1)	(2)	(3)	(4)	(5)	(6)	(7)
inner	$5.9 \times 10^{65}$	$1.2 \times 10^{-2} f^{-1/2}$	$3.0 \times 10^{-11} f^{-1/2}$	$6.8 \times 10^6 f^{1/2}$	$2.6 \times 10^{55} f^{1/2}$	$5.2 \times 10^8 f^{1/2}$
outer	$7.3 \times 10^{67}$	$1.0 \times 10^{-3} f^{-1/2}$	$2.7 \times 10^{-12} f^{-1/2}$	$6.4 \times 10^7 f^{1/2}$	$2.9 \times 10^{56} f^{1/2}$	$5.8 \times 10^9 f^{1/2}$



## REFERENCES

- Armus, L., Heckman, T.M., Weaver, K.A., and Lehnert, M.D. 1995, *ApJ*, 445, 666.
- Arnaud, K.A. 1996, *ASP Conf.Series*, 101,17.
- Bland-Hawthorn, J., *Publ.Astron.Soc.Aust.*, 12, 190.
- Della Ceca, R., Griffiths, R.E., Heckman, T.M., and MacKenty, J.W. 1996, *ApJ*, 469, 662.
- Della Ceca, R., Griffiths, R.E., Heckman, T.M., 1997, *ApJ*, 485, 581.
- de Vaucouleurs, G., de Vaucouleurs, A., Corwin, H. Buta, R., Paturel, R., and Fouque, P.  
1991, *Third Reference Catalog of Bright Galaxies* (Austin: Univ. Texas Press).
- Dahlem, M., Weaver, K.A., and Heckman, T.M. 1998, *ApJS*, in press.
- Dotani, T., et al., 1996, *ASCA News*, 4, 3.
- George, I.M., Arnaud, K.A., Pence, B., and Ruamsuwan, L. 1992, *Legacy*, 2, 51.
- Heckman, T.M., Lehnert, M.D., and Armus, L. 1993, in *The Evolution of Galaxies and  
Their Environments*, ed. S.M. Shull and H. Thronson (Dordrecht: Kluwer), 455.
- Lehnert, M.D., and Heckman, T.M. 1995, *ApJS*, 97, 89.
- Lehnert, M.D., and Heckman, T.M. 1996, *ApJ*, 462, 651.
- Lisenfeld, U., Alexander, P., Pooley, G.G., and Wilding, T. 1996, *MNRAS*, 281, 301.
- Moffet, A.T. 1975 in *Stars and Stellar System*, vol. IX: *Galaxies and the Universe*, eds  
A.Sandage, M.Sandage and J.Kristian (University of Chicago Press:Chicago),p. 211.
- Moran, E.D., and Lehnert, M.D. 1997, *ApJ*, 478, 172.

Nagase, F., 1989, PASJ, 41, 1.

Persic, M., et al., 1998, astro-ph/9809256.

Ptak, A., Serlemitsos, P., Yaqoob, T., Mushotzky, R., and Tsuru, T. 1997, AJ, 113, 1286.

Suchkov, A.A., Balsara, D.S., Heckman, T.M., and Leitherer, C. 1994, ApJ, 430, 511.

Tanaka, Y., Inoue, H., and Holt, S.S. 1994, PASJ, 46, L37.

Tanaka, Y., 1996, MPE Report, 263, 85.

White, R.L., et al. 1992, ApJS, 79, 331.

Zezas, A.L., Georgantopoulos, I., and Ward, M.J. 1998, astro-ph/9807258

## 6. Figure Captions

Figure 1: Residuals to the best fit Raymond-Smith model. G23: open squares; S01: filled squares. For this plot, the spectra have been rebinned so that the signal-to-noise ratio in each channel is at least 3.

Figure 2: The folded spectrum and the residuals of the GIS2+GIS3 data set compared with the best fit Raymond-Smith plus Power Law model. For this plot, the spectra have been rebinned so that the signal-to-noise ratio in each channel is at least 3.

Figure 3: The folded spectrum and the residuals of the SIS0+SIS1 data set compared with the best fit Raymond-Smith plus Power Law model. For this plot, the spectra have been rebinned so that the signal-to-noise ratio in each channel is at least 3.

Figure 4: The unfolded spectrum of the ASCA + ROSAT PSPC data set (Ray+Po model). For this plot, the spectra have been rebinned so that the signal-to-noise ratio in each channel is at least 3.

NGC 2146 (G23 + S01 data)

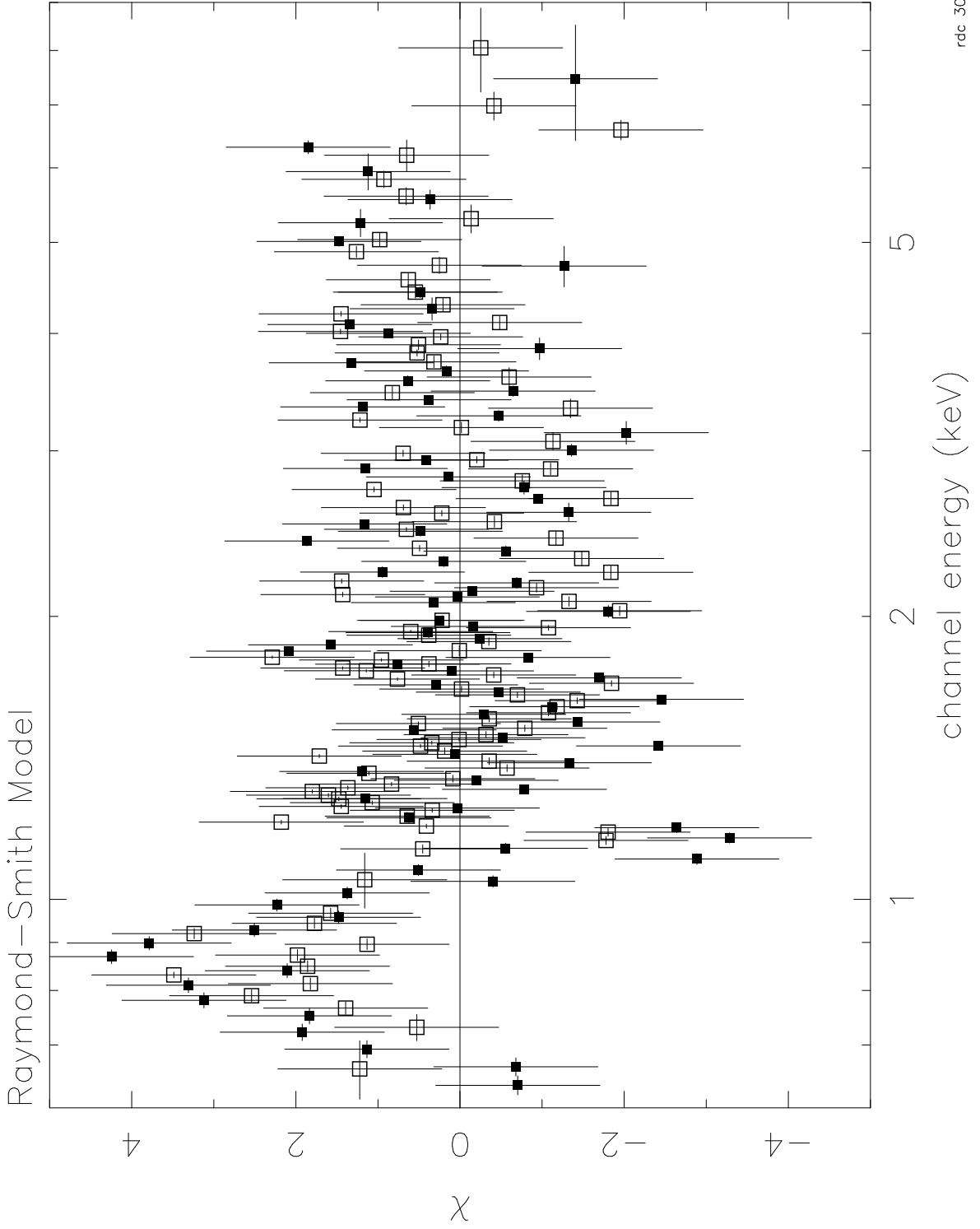


Fig. 1.—

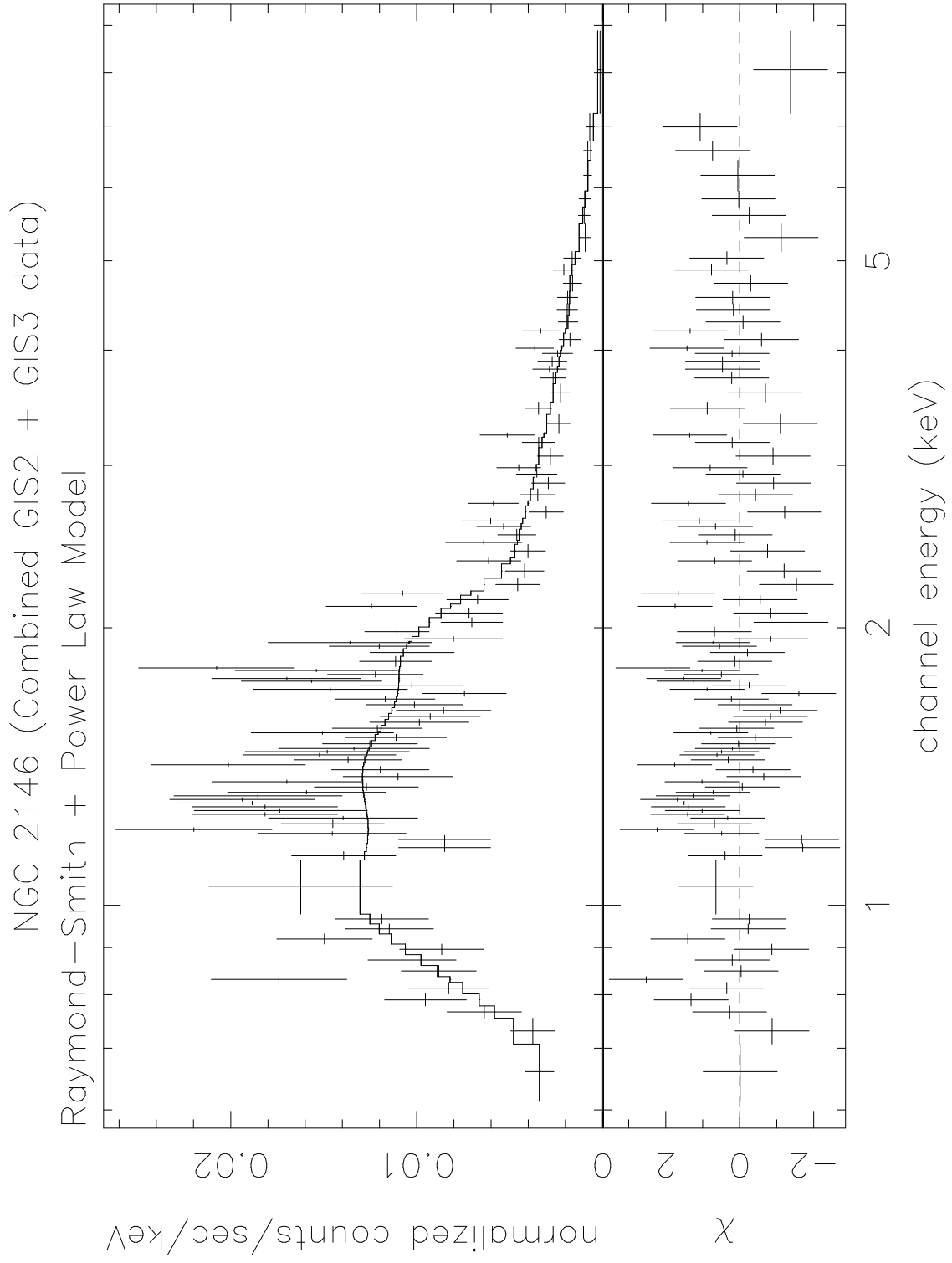


Fig. 2.—

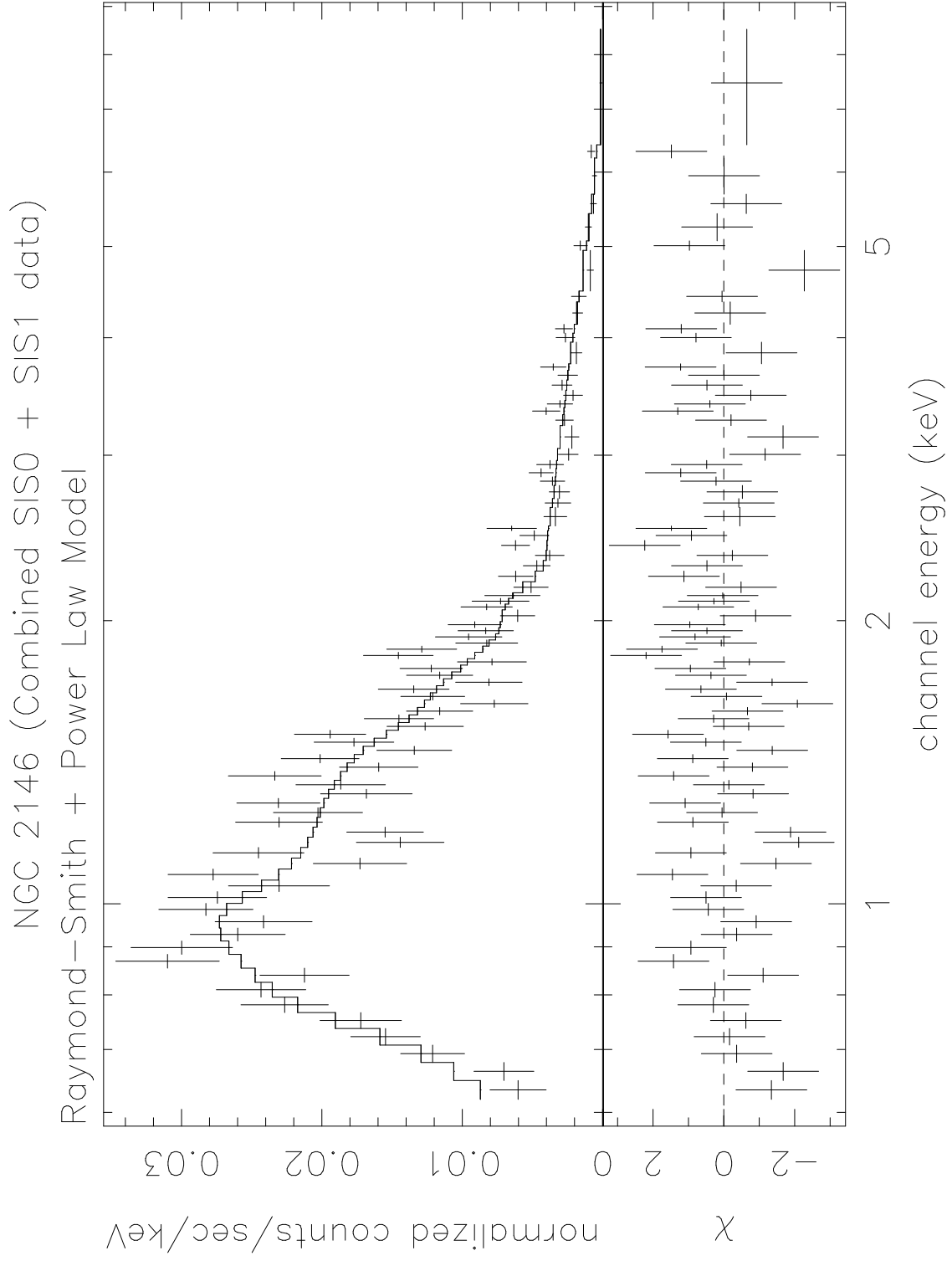


Fig. 3.—

